APSB
Acta Pharmaceutica Sinica B
2021
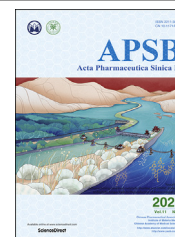
ORIGINAL ARTICLE

Norlichexanthone purified from plant endophyte prevents postmenopausal osteoporosis by targeting ERα to inhibit RANKL signaling

Keqi Wang[a], Yongyan Chen[a], Shuo Gao[a], Maosi Wang[a], Mengmeng Ge[a], Qian Yang[a], Mingkai Liao[a], Lin Xu[a], Junjie Chen[a,b], Zhiping Zeng[a,b], Haifeng Chen[a], Xiao-kun Zhang[a,b], Ting Lin[a,*], Hu Zhou[a,b,*]

[a]*School of Pharmaceutical Sciences, Fujian Provincial Key Laboratory of Innovative Drug Target Research, Xiamen University, Xiamen 361102, China*
[b]*High Throughput Drug Screening Platform, Xiamen University, Xiamen 361102, China*

Abstract   Although different types of drugs are available for postmenopausal osteoporosis, the limitations of the current therapies including drug resistances and adverse effects require identification of novel anti-osteoporosis agents. Here, we defined that norlichexanthone (NOR), a natural product, is a ligand of estrogen receptor-alpha (ERα) and revealed its therapeutic potential for postmenopausal osteoporosis. We used mammalian-one hybrid assay to screen for ERα modulators from crude extracts of several plant endophytes. As a result, NOR purified from the extract of endophyte ARL-13 was identified as a selective ERα modulator. NOR directly bound to ERα with an affinity in nanomolar range, revealing that it is a natural ligand of ERα. NOR induced osteoblast formation in MC3T3-E1 precursor cells. Conversely, NOR inhibited receptor activator of nuclear factor-kappa B ligand (RANKL)-induced osteoclast formation in both RAW264.7 macrophages and mouse primary monocytes. Mechanistically, NOR inhibited RANKL-induced association of ERα and TRAF6 to prevent ERα-mediated TRAF6 activation *via* Lys63-linked ubiquitination. Importantly, NOR exhibited potent anti-osteoporosis efficacy in an ovariectomized mouse model. Comparing to estrogen, NOR was of much less capability in stimulating endometrial hyperplasia and promoting mammalian cancer cell proliferation. Taken together, our study identified NOR as a natural and high affinity ligand of ERα with substantial anti-osteoporosis but less estrogenic activity.

*Corresponding authors. Tel.: +86 592 2881105; fax: +86 592 2881105.
E-mail addresses: huzhou@xmu.edu.cn (Hu Zhou), linting@xmu.edu.cn (Ting Lin).

1. Introduction

Estrogen receptor-alpha (ERα) belonging to nuclear receptor superfamily plays vital and variety roles in pathophysiological processes[1−4]. Particularly, the dysfunction of ERα is highly related to breast, ovary and endometrial cancers[5]. The activities of ERα are tightly regulated by its cognate ligands that generally bind to the ligand binding domain (LBD) of ERα[6]. Besides the three major endogenous estrogens, *i.e.*, estrone (E_1), estradiol (E_2) and estriol (E_3), many natural and synthetic products were identified as ERα ligands[7,8]. Several ERα ligands including agonists and antagonists are widely used as clinical drugs. For example, tamoxifen and raloxifene are used for treating breast cancers and postmenopausal osteoporosis[9,10].

Postmenopausal osteoporosis results from the loss of estrogen due to the functional failure of ovaries[11,12]. Bone remodeling is a dynamic process of bone resorption by osteoclast and bone formation by osteoblast. One major pathological mechanism of osteoporosis is the imbalance of the functions of osteoblast and osteoclast, leading to the abnormal bone remodeling[13]. Estrogen is an essential factor to promote osteoblast but inhibit osteoclast formation, rendering the functional balance of osteoblast and osteoclast[14−16]. Although clinical drugs are available for treating postmenopausal osteoporosis, they are often associated with severe side effects[17−19]. Osteoclast inhibitors, such as bisphosphonates, may cause excessive suppression of bone turnover, resulting in low-trauma, atypical fractures, esophagitis and atrial fibrillation[20]. Hormone replacement therapy (HRT), such as estrogen treatment, is effective to prevent postmenopausal osteoporosis[21,22]. However, estrogen treatment often increases the risk of endometrial, ovarian and mammary carcinoma, resulting from its strong estrogenic activity[23]. Thus, discovering novel ERα ligands with less estrogenic activity but strong anti-osteoporosis effect will improve the benefit of ERα-targeted drugs in postmenopausal osteoporosis treatment.

Osteoclasts are fully differentiated, multi-nucleated cells originating from the hematopoietic monocyte-macrophage linage[24,25]. Receptor activator of nuclear factor-kappa B ligand (RANKL) is a key factor for inducing osteoclast formation[26]. RANKL binds to its cognate receptor RANK on the plasma membrane to initiate downstream signaling cascade, including activation of mitogen activated protein kinases (MAPKs), nuclear factor kappa B (NF-κB) and the phosphatidylinositol 3-kinase (PI3K) pathways[27,28]. The receptor RANK lacks intrinsic kinase activity and requires the recruitment of TNF receptor associated factors (TRAFs) to transduce signaling[29]. TRAF6-deficient mice showing defective osteoclastogenesis and severe osteopetrosis indicate the essential role of TRAF6 in osteoclast formation and in RANKL signaling[30,31]. TRAF6 is an E3 ubiquitin ligase and can catalyze itself Lys63-linked ubiquitination, which is essential for transducing RANKL signal[24]. Estrogen has been implicated in the regulation of RANKL signaling, whereas the underlying mechanism is obscure[32].

Plant endophytes are an endosymbiotic group of microorganisms that colonize in plants. They are reservoirs of numerous and novel bioactive secondary metabolites with diverse structures[33,34]. Many natural active products including clinical drugs are obtained or derived from plant endophytes[35]. In this study, we identified compound norlichexanthone (NOR) purified from a plant endophyte as an active ERα ligand. Furthermore, we unraveled that NOR is of potent therapeutic effect on postmenopausal osteoporosis by inducing osteoblast formation but inhibiting osteoclast formation. Moreover, we disclosed that NOR inhibits RANKL signaling by inhibiting ERα-mediated Lys63-linked ubiquitination of TRAF6, resulting in inhibition of osteoclast formation. Importantly, NOR is of much less estrogenic activity than E_2.

2. Materials and methods

2.1. Reagents and antibodies

NOR (98% purity) was isolated and obtained according to the procedure depicted, dissolved in dimethyl sulfoxide (DMSO) and stored at −20 °C. 17β-Estradiol (E_2), 9-*cis* retinoic acid (9-*cis*-RA), all-*trans* retinoic acid (ATRA), β-glycerophosphate and L-ascorbic acid were purchased from Sigma (St. Louis, MO, USA), and ICI-182780 was from MedChemExpress (Monmouth Junction, NJ, USA). Endoxifen and 4-[2-phenyl-5,7-bis(trifluoromethyl)pyrazolo[1,5-*a*]pyrimidin-3-yl]phenol (PHTPP) were from Target Mol (Boston, MA, USA). Recombinant murine RANKL was purchased from Abcam Systems (Cambridge, MA, USA) and macrophage colony-stimulating factor (M-CSF) was from PeproTech (Cranbury, NJ, USA). Transfection reagent linear polyethylenimine (PEI) used to transfect HEK293T cells was purchased from Polysciences (Warrington, PA, USA). Reverse transcription reagents and SYBR Green PCR Master Mix were from Yeasen (Shanghai, China). Specific primary antibodies against TRAF6, ERα, MYC, ubiquitin, ERK, JNK were purchased from Santa Cruz Biotechnology (Dallas, TX, USA). Antibodies for phospho-P44/42 MAPK (ERK1/2), phospho-SAPK/JNK (Thr183/Tyr185), phospho-P38 MAPK (Thr180/Tyr182) and P38 MAPK were obtained from Cell Signaling Technology (Danvers, MA, USA). Antibodies for β-actin and Flag were purchased from Sigma, and anti-ubiquitin (linkage-specific K63) was from Abcam. HRP-conjugated secondary antibodies against rabbit IgG and mouse IgG were purchased from Thermo Fisher Scientific (Waltham, MA, USA). The ALP activity assay kit, and cell lysis buffer for Western and IP were from Beyotime Biotechnology (Shanghai, China). The TRAP staining kit was purchased from Leagene (Beijing, China).

2.2. Cell source and culture

The MC3T3-E1 and bone marrow monocytes were cultured in minimum essential medium Eagle-alpha modification (α-MEM) supplemented with 10% fetal bovine serum (FBS) in a humidified atmosphere containing 5% CO_2 at 37 °C, while RAW264.7, MCF-7, MDA-MB-231 and HEK293T cells were cultured in Dulbecco's modified Eagle medium (DMEM). Bone marrow monocytes were

isolated from 6 to 8 weeks old C57BL/6 mice. In brief, the mice were sacrificed by anesthesia and immersed in 70% ethanol for 5 min, and then the femur and tibia were separated. The α-MEM medium was pipetted with a syringe to flush the bone marrow cavity, and the flushed medium was centrifuged at 1400 rpm (Centrifuge 5424 R, Eppendorf, Hamburg, Germany) for 5 min at room temperature to collect cells. Erythrocyte lysate (#555899, BD company, Franklin Lake, NJ, USA) was used to remove erythrocytes, and the cells were cultured in medium with M-CSF (50 ng/mL) overnight. The suspension cells were collected and then resuspended in α-MEM containing M-CSF (50 ng/mL) and RANKL (50 ng/mL) for osteoclast induction.

2.3. Mammalian one-hybrid assay

HEK293T cells were co-transfected with pG5-luciferase reporter (Promega, Madison, WI, USA) together with the recombinant pBIND plasmids encoding ligand binding domain (LBD) of nuclear receptors fused with the DNA-binding domain (DBD) of Gal4. One day after transfection, cells were treated with DMSO, NOR or ligands specific for each nuclear receptor. After 12 h, cells were lysed by passive lysis buffer. Firefly and *Renilla* luciferase activities were quantitated using the Dual-Luciferase Reporter Assay System (Promega, E1960). *Renilla* luciferase values were normalized to firefly luciferase activity and plotted as relative luciferase activity.

2.4. Fluorescence titration assay

The fluorescence titration assay was performed as previously described[36,37]. The ERα/LBD protein was dissolved in phosphate-buffered saline (PBS) at a concentration of 2.5 μmol/L, and the protein solution was stabilized to room temperature. Protein solution (3 mL) was transferred to the cuvette. The excitation wavelength of the instrument was set to 280 nm and the emission wavelength was set between 300 and 500 nm. The excitation and emission slit width was set to 5 nm. The compounds were then added dropwise to the cuvette, and the fluorescence spectrum of each titration was recorded. The compound concentration was the abscissa, and the change in spectroscopic signal after each titration was plotted as the ordinate. K_d value was obtained by Eq. (1) using Origin software (OriginLab, Northampton, MA, USA):

$$y = C(x + P + K_d)/2 - C \times \text{sqrt}\left((x + P + K_d)^2 - 4Px\right)/2 \qquad (1)$$

in which y represents the change of fluorescence intensity after each titration, x represents compound concentration, P represents protein concentration (P is 2.5 μmol/L here), C is a constant which measure the change in signal (ΔF) changes per unit complex (ligand−protein) concentration (molar signal coefficient).

2.5. Differential scanning calorimetry (DSC)

Calorimetric measurements were performed using the VP-DSC (GE Healthcare, Fairfield, CT, USA). The VP-DSC was run without feedback and 15−30 min equilibration times at 10 °C were used before or between scans. The ERα/LBD protein samples were concentrated to 2.5 mg/mL in PBS. The proteins were scanned from 10 to 100 °C at a heating rate of 90 °C/h. A cuvette containing PBS was used as a reference. DSC data was corrected for PBS base lines and normalized for scan rate and protein concentration[38].

2.6. Computer-aided docking

Computational docking of E_2 and NOR with ERα was initially performed in order to be used as internal control for comparative scoring purpose. The initial dockings were carried out in Maestro 11.1 (Schrödinger, New York, NY, USA). The 3D structure of ERα (PDB 1ERE) was downloaded from the Research Collaboratory for Structural Bioinformatics Protein Data Bank (RCSB PDB). Here, the receptor grid files were generated covering the active site region with van der Waals radius scaling of 1.0 Å to soften the non-polar region of receptor and the other atoms were left free of scaling. Ten energetically favorable conformations were selected out of per docking. Among them, the best pose in terms of significant docking score was picked.

2.7. Osteoblast formation

MC3T3-E1 cells were seeded in a 24-well plate, and treated with a mineralization-inducing solution containing 10 mmol/L β-glycerophosphate and 50 μg/mL ascorbic acid. The cells were continuously cultured for 14 days, and the medium was changed every 2 days. Differentiated cells were stained with alizarin red staining at the indicated day. Cells were gently rinsed twice with PBS, fixed with 4% paraformaldehyde for 10 min, then washed twice with double distilled water. Cells were stained with 1% alizarin red S staining solution at 37 °C for 30 min, then washed with distilled water. The alizarin red staining was then visualized and photographed. When detecting ALP activity, the cells were lysed and the supernatant was used to determine the activity by the ALP detection kit (Beyotime Biotechnology) according to the manufacturer's instructions.

2.8. Osteoclast formation

Bone marrow monocytes were cultured for 7 days in the presence of M-CSF (50 ng/mL) and RANKL (50 ng/mL) for differentiation into mature osteoclasts. Media was refreshed every 2 days. RAW264.7 cells were seeded in 6-well plates in full medium containing RANKL (50 ng/mL) for 7 days as well. For tartrate-resistant acid phosphatase (TRAP) staining, cells were fixed and stained for TRAP activity. TRAP-positive multi-nucleated cells with ≥3 nuclei were counted as osteoclasts.

2.9. Cell proliferation and viability assay

MC3T3-E1 and RAW264.7 cells were seeded respectively into 96-well plates at the density of 5×10^3 cells/well in full medium with vehicle or corresponding differentiation-inducing agents medium. MCF-7 cells were plated at the concentration of 8×10^3 cells/well followed by 48 h incubation. The plates were incubated at 37 °C for 4 h after 10 μL of 3-(4,5-dimethylthiazol-2-yl)-2,5-diphenyltetrazolium bromide (MTT, 5 mg/mL) per well was added, and then the supernatant was removed. DMSO (150 μL) was added to dissolve the crystals on the oscillator for 10 min. The absorbance at 490 nm was measured by the plate reader.

2.10. Quantitative real-time PCR

Chiefly, total RNA was isolated using Trizol reagent (Life) according to the manufacturer's recommended protocol, and then 1 μg of RNA was used for cDNA synthesis with Revert Aid First Strand cDNA Synthesis Kit (Yeasen). Real-time PCR in triplicate

was performed with SYBR Green Master Mix (Yeasen) on AriaMx real-time PCR System (Agilent, Santa Clara, CA, USA). All values were reported as the mean ± standard deviation (SD) of triplicate measurements of each cDNA sample. The mRNA levels were normalized to *Gapdh* mRNA. PCR primers used were as followed: mouse cathepsin k, forward 5′-ACGAGAAAG CCCTGAAGA-3′, and reverse 5′-TGTAAAACTGGAAAGATG CC-3′; mouse *Nfatc1*, forward 5′-ACCACCTTTCCGCAACCA-3′, and reverse 5′-TTCCGTTTCCCGTTGCA-3′; and *Gapdh*, forward 5′-AAGAAGGTGGTGAAGCAGG-3′ and reverse 5′-GAAGGTGGAAGAGTGGGAGT-3′.

2.11. Ovariectomized mice model

C57BL/6J female mice were purchased from Shanghai SLAC laboratory animal company. Mice were housed under standard conditions (temperature, 22 °C; humidity, 40%−60%; light, 12 h of light/dark cycle; and pathogen-free-controlled environment). Food and water were available *ad libitum*. Mice received bilateral ovariectomy (OVX) or sham operation (Sham) at 10-week old. Two weeks after surgery, the mice were randomly divided into 4 groups with 6 mice/group: vehicle-treated sham-operated (Sham + Veh), vehicle-treated OVX (OVX + Veh), NOR (1 mg/kg)-treated OVX (OVX + NOR) and E$_2$ (1 mg/kg)-treated OVX (OVX + E$_2$). NOR was administered orally for 8 weeks, while sham group and OVX control group were given with 0.5% CMC-Na. Mice were euthanized and their femurs and vertebras were dissected and collected. Bones were fixed in formalin for at least 48 h. The right femurs and 5th vertebras were scanned *ex vivo* using a micro-computed tomography (μ-CT) system (SKYSCAN 1272, Bruker, Belgium). The parameters of the μ-CT system were set as follows: source voltage, 70 kV; source current, 142 μA; scaling image pixel size, 11.199 μm; the filter, 0.5 mm. After the 3D reconstruction by InstaRecon (Belgium), we set the first section of cross from butterfly cut where started from the distal end of the femur, and then counted 50th to 200th section. Lastly, we used CTAn software to analysis the data of femoral and vertebral cancellous bone. For quantitative assessment, the bone parameters such as bone mineral density (BMD), bone volume/tissue volume (BV/TV) and trabecular bone number (Tb.N) were calculated with scanner software according to standardized protocols.

2.12. Western blotting and co-immunoprecipitation

Cells were lysed using cell lysis buffer (Beyotime Biotechnology) and centrifuged for 15 min at 4 °C followed by collection of the supernatant. After quantified by a BCA protein assay kit (Thermo Fisher Scientific), equal amounts of protein were loaded onto and separated by (8%−10%) SDS-PAGE gels and transferred to PVDF membranes. Membranes were blocked with 5% nonfat milk for 1 h. The blots were probed with correspondent specific primary antibodies at 4 °C overnight, followed by the secondary HRP conjugated anti-mouse/rabbit antibodies at room temperature for 2 h. After washing, the bands were detected by chemiluminescence and imaged. For co-immunoprecipitation (Co-IP), antibodies were added to the supernatant of cell lysis and the mixture was incubated at 4 °C overnight, and then IgG agarose beads were added and incubated for 3 h. The beads were isolated by centrifugation with 3000 rpm (Centrifuge 5424 R, Germany) for 5 min and washed three times with prechilled PBS, followed by protein denaturation at 100 °C for 5 min and Western blotting analysis.

2.13. Cell cycle analysis

Briefly, cells were collected and washed twice with prechilled PBS, then fixed with 70% ethanol at 4 °C overnight. The cells were incubated with DAPI (sigma) in the dark at room temperature for 10 min, then analyzed using Flow Cytometers.

2.14. TRAP staining analysis of lumbar vertebra osteoclast activity

The 5th lumbar vertebra (L5) of the mice was extracted, fixed at 4% paraformaldehyde at 4 °C for 24 h, and the non-decalcified bones were embedded in methyl methacrylate. Sections (5 μm thick) were obtained by a microtome (RM2255, Leica Microsystems, Wetzlar, Germany) and Leica TC65 microtome blade (14021626379, Leica Microsystems). For static histomorphometric measures of osteoclast parameters, undecalcified sections of the vertebra were stained using TRAP staining kit (G1492, Solarbio, Beijing, China). The Osteomeasure Analysis System (OsteoMetrics, Atlanta, GA, USA) was used for bone histomorphometry using standard procedures according to the program's instruction.

2.15. Animal study approval

All animal experiments complied with the National Institutes of Health guide for the care and use of Laboratory animals and were approved by the Animal Experiment Administration Committee of Xiamen University in Fujian, China.

2.16. Statistical analysis

Data were expressed as the mean ± SD. Each assay was repeated in triplicate in three independent experiments. The statistical analyses were performed using GraphPad Prism 8 software. The statistical significance of the differences among the means of several groups was determined using the Student's *t* test. Level of statistical significance was determined as $P < 0.05$.

3. Results

3.1. Norlichexanthone selectively activates ERα

To explore the potential ligands of ERα from plant endophytes, we used ERα mammalian one-hybrid assay to evaluate the crude extracts of several plant endophytes. Among the 6 endophytes examined, the crude extract from endophyte ARL-13, similar as ERα agonist 1,3,5-tris (4-hydroxyphenyl)-4-propyl-1*H*-pyrazole (PPT)[39], robustly transactivated Gal4/DBD-ERα/LBD fusion protein (Supporting Information Fig. S1A and S1B). The sequence of internal transcribed spacer (ITS) indicated that ARL-13 belonged to *Arthrinium arundinis* genus (Supporting Information Fig. S2A and S2B). The result that ARL-13 extract strongly transactivated the Gal4 chimers of ERα but not RARα, RARγ or RXRα indicated the selectivity of the extract in ERα regulation (Supporting Information Fig. S3). These results indicate that ARL-13 extract contains substances that regulate ERα transcriptional activity.

The extract of ARL-13 underwent further separation and purification by silica gel column chromatography and pre-HPLC (Supporting Information Fig. S4), and several compounds were

obtained, of which compound **1** potently activated Gal4/DBD-ERα/LBD (Fig. 1A). After examination by ^{1}H and ^{13}C NMR spectroscopy and mass spectrometry (Supporting Information Figs. S5−S7), compound **1** was identified as norlichexanthone (NOR, Fig. 1B). We found that NOR dose-dependently activated Gal4/DBD-ERα/LBD with an EC$_{50}$ of 38.81 nmol/L (Fig. 1C). Nevertheless, the efficacy of NOR on activating ERα was much weaker than 17β-estradiol (E$_{2}$, Fig. 1C). As expected, NOR selectively activated ERα but not RARα, RXRα or PPARγ (Fig. 1D). Taken together, these results indicate that compound NOR from plant endophyte is a selective modulator of ERα transactivation.

3.2. NOR binds to ERα

To further characterize NOR as an ERα modulator, we explored whether NOR directly bound to ERα. The result of differential scanning calorimetry (DSC) assay shows that NOR potently increased not only the melting temperature (T_{m}) but also the melting energy of ERα/LBD protein (Fig. 2A). This result suggests that NOR binds to ERα to enhance its thermostability. We further used fluorescence titration assay to determine NOR binding to ERα. We found that NOR dose-dependently reduced the fluorescence intensity of ERα/LBD but not RXRα/LBD (Fig. 2B and C), while the fluorescence of ERα/LBD was not affected by RXRα ligand K-80003 (Fig. 2D). These results indicate that NOR binds to ERα selectively. The K_{d} value of NOR and ERα interaction obtained by the fluorescence titration assay was 10 nmol/L (Fig. 2B), and was of the same order of magnitude with the EC$_{50}$ of NOR transactivating ERα. Together, these results indicate that NOR is a natural ligand of ERα.

We further used computer-aided docking approaches to examine the binding mode of NOR−ERα. Our computational modeling indicated that NOR and E$_{2}$ had similar ERα binding mode (Fig. 2E). The hydroxyl group of NOR at site 3 formed hydrogen bond with His524 amino acid residue in the ligand binding pocket (LBP) of ERα, while the hydroxyl group at site 6 formed hydrogen bonds with Glu353 and Arg394 residues of ERα (Fig. 2E). Thus, the hydroxyl groups at 3 and 6 sites should be essential for NOR binding to ERα. The hydrogen bond formed between hydroxyl group of NOR and Arg394 was longer than the corresponding one formed between E$_{2}$ and Arg394 (Fig. 2E), which may lead to the differences of NOR and E$_{2}$ in regulating ERα activities.

3.3. NOR induces osteoblastic differentiation

In view of the fact that NOR was ERα ligand, we investigated whether NOR could induce osteoblastic differentiation as estrogen does[40]. Calcium deposits is an indication of successful osteoblast formation *in vitro* and can specifically be stained bright red by Alizarin Red S[41]. Mineralization-inducing solution induced calcium deposits in MC3T3-E1 cells, which was potently enhanced by NOR and E$_{2}$ at 20 nmol/L concentration (Fig. 3A). This indicates that NOR and E2 could strengthen the effect of the inducing solution on osteoblastic induction. Importantly, NOR appeared to induce more calcium deposits than E$_{2}$ at the same concentration (Fig. 3A). Consistently, NOR potently increased the activity of alkaline phosphatase (ALP), a marker of osteoblast[42], in induced MC3T3-E1 cells (Fig. 3B). NOR treatment did not show significant effect on the proliferation of MC3T3-E1 cells (Fig. 3C), indicating that the increased calcium accumulation

induced by NOR did not result from cell proliferation and most likely resulted from the osteoblastic induction.

3.4. NOR inhibits osteoclast formation

We then explored whether NOR affected osteoclast formation as well. Murine macrophage RAW264.7 cells were osteoclast precursors and can be induced differentiation into osteoclast by RANKL[25]. In the absence of RANKL treatment, RAW264.7 cells were small and round cells with single nucleus. After RANKL treatment, large multi-nucleated cells emerged and were stained red by TRAP staining, indicating the occurrence of osteoclast formation (Fig. 4A). E$_{2}$ has been reported to inhibit osteoclast formation, which was corroborated in our result showing that E$_{2}$ dose-dependently reduced the numbers of multi-nucleated cells (Fig. 4A). NOR also significantly reduced the numbers of multi-nucleated cells with the comparable ability as E$_{2}$ (Fig. 4A). The effect of NOR on osteoclast formation was also evaluated using the primary monocytes purified from murine marrow. As shown in Fig. 4B, RANKL-induced large multi-nucleated cell formation from the primary monocytes was potently inhibited by either NOR or E$_{2}$. Moreover, NOR and E$_{2}$ inhibited RANKL-stimulated mRNA expression of cathepsin k and *Nfatc-1*, two marker genes of osteoclasts[43−45] (Fig. 4C). In the absence of RANKL, NOR and E$_{2}$ had no apparent effect on RAW264.7 cell viability (Fig. 4D). However, they potently inhibited RAW264.7 cell viability in a dose-dependent manner when cells were pretreated with RANKL (Fig. 4E). These data indicate that NOR inhibited the survival of RANKL-induced osteoclast but not the precursor RAW264.7 cells. In sum, these data indicate that NOR inhibits osteoclast formation from osteoclast precursors.

3.5. NOR inhibits RANKL signaling by preventing ERα-induced TRAF6 ubiquitination

Furthermore, we explored the underlying mechanism of NOR actions in osteoclastogenesis. The master transcriptional factor inducing osteoclastic differentiation is NFATc1, which is induced by transcriptional factor AP-1, a heterodimer of c-JUN and c-FOS[29]. AP-1 is regulated by the c-JUN N-terminal kinase (JNK), P38 and extracellular signal-regulated kinase (ERK) MAPKs, downstream of RANKL signaling[29,43]. The downregulation of RANKL-induced *Nfatc1* mRNA expression by NOR and E$_{2}$ suggested that they may inhibit RANKL signaling (Fig. 4C). Indeed, both NOR and E$_{2}$ dose-dependently inhibited RANKL-induced phosphorylation of JNK, P38 and ERK but not their expression in RAW264.7 cells (Fig. 5A). Thus, NOR and E$_{2}$ were inhibitors of RANKL signaling. ICI-182780 (fulvestrant) is an antagonist of ER[40,46]. Interestingly, the inhibitory effect of NOR and E$_{2}$ on RANKL-induced JNK activation was blocked by fulvestrant (Fig. 5B). To further characterize ERα or ERβ dependent effects of NOR, we used the ERα selective antagonist endoxifen[47] and the ERβ selective antagonist PHTPP[48]. Endoxifen but not PHTPP substantially abrogated the effect of NOR and E$_{2}$ on RANKL-induced JNK activation (Fig. 5C). These data indicate the ERα-dependent effect of NOR and E$_{2}$ on inhibiting RANKL signaling.

In the RANKL signaling pathway, RANK-triggered ubiquitination of TRAF6 initiates the activation of downstream signal cascades[24]. The triggered auto-ubiquitination of TRAF6 *via* a Lys63-linked polyubiquitin chain mediates the recruitment of TAK1 binding protein 2 (TAB2), leading to TAK1 activation and
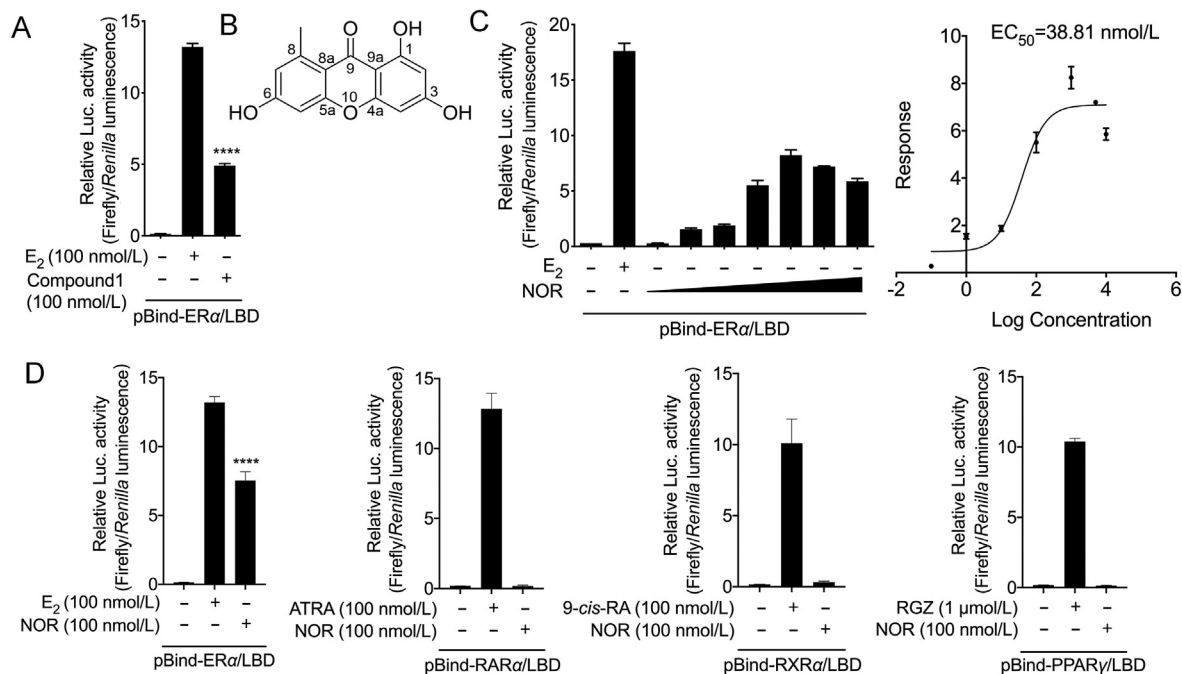
Figure 1 NOR selectively activates the transcriptional activity of ERα. (A) HEK293T cells transfected with pBind-ERα/LBD and pG5-luciferase plasmids were treated with E_2 (100 nmol/L) or compound **1** (100 nmol/L) for 12 h. Cells were harvested, and firefly and *Renilla* luciferase activities were measured. *Renilla* luciferase values were normalized to firefly luciferase activity and plotted as relative luciferase (Luc.) activity. (B) The chemical structure of NOR. (C) HEK293T cells transfected with pBind-ERα/LBD and pG5-luciferase plasmids were treated with E_2 (10 nmol/L) or NOR (1, 10, 20, 40, 60, 80, and 100 nmol/L). Luciferase activities were measured and plotted. (D) The effects of NOR on transactivating the chimers of Gal4/DBD fused with the LBD of ERα, RARα, RXRα or PPARγ. E_2, 17β-estradiol; ATRA, all-*trans* retinoic acid; 9-*cis*-RA, 9-*cis* retinoic acid; RGZ, rosiglitazone. Data are expressed as the mean $\pm$ SD; ****$P < 0.0001$ by Student's *t* test.

in turn the phosphorylation of MKK[49]. We found that ectopically expressed ERα potently induced the Lys63-linked ubiquitination of TRAF6 in HEK293T cells (Fig. 5D). Interestingly, ERα-induced ubiquitination of TRAF6 was inhibited by either NOR or E_2 (Fig. 5D). These data suggest that NOR and E_2 antagonize RANKL signaling through inhibiting ERα-induced TRAF6 ubiquitination. Moreover, the ectopically expressed ERα interacted with TRAF6, which was inhibited by NOR and E_2 in a dose-dependent manner (Fig. 5E). In addition, RANKL induced the endogenous interaction of ERα and TRAF6 in RAW264.7 cells, which was also inhibited by either NOR or E_2 (Fig. 5F). Together, these data suggested that ERα binds and then induces TRAF6 ubiquitination while NOR and E_2 inhibit RANKL-induced interaction of ERα and TRAF6 to exert their inhibitory effect on RANKL signaling (Fig. 5G).

3.6. NOR prevents osteoporosis in a mouse postmenopausal osteoporosis model

To evaluate the potential efficacy of NOR in osteoporosis, we used an ovariectomized (OVX) mouse model, a well-established model of estrogen deficiency-mediated osteoporosis[50]. After ovariectomized operation, mice were oral gavaged with NOR and E_2 daily for 8 weeks, respectively. Right femurs were obtained and subjected to μ-CT analysis of the trabecular architecture. As shown in

Fig. 6A, the structure of trabecular of distal femurs was severely impaired in OVX mice comparing to control (Sham) mice. The bone mineral density (BMD), bone volume density (BV/TV) and trabecular number (Tb.N) were largely reduced in OVX mice comparing to sham mice (Fig. 6A). These results indicate the success of our OVX model in bone loss. Notably, NOR or E_2 at the dosage of 1 mg/kg potently prevented the ovariectomy-induced deterioration of trabecular architecture (Fig. 6A). The ovariectomy-induced reduction of BMD, BV/TV and Tb.N were inhibited by NOR or E_2 treatment (Fig. 6A). Similar result was obtained in the fifth vertebras of mice (Fig. 6B). Moreover, the ovariectomy-induced osteoclast formation in vertebras was inhibited by NOR or E_2 (Fig. 6C). Therefore, NOR showed strong efficacy in osteoporosis prevention in an OVX mouse model.

3.7. NOR is of weak estrogenic activity

One of the major adverse effects of using estrogen for osteoporosis treatment is the increased risk for endometrial hyperplasia and breast cancer promotion originating from its strong estrogenic activity[23]. One of the estrogenic effects is manifested in maintaining uterus morphology and function[51]. In our OVX mouse model, we observed the significant shrinkage and weight reduction of uterus (Fig. 7A and Supporting Information Fig. S8A), resulting from the lack of estrogen due to the
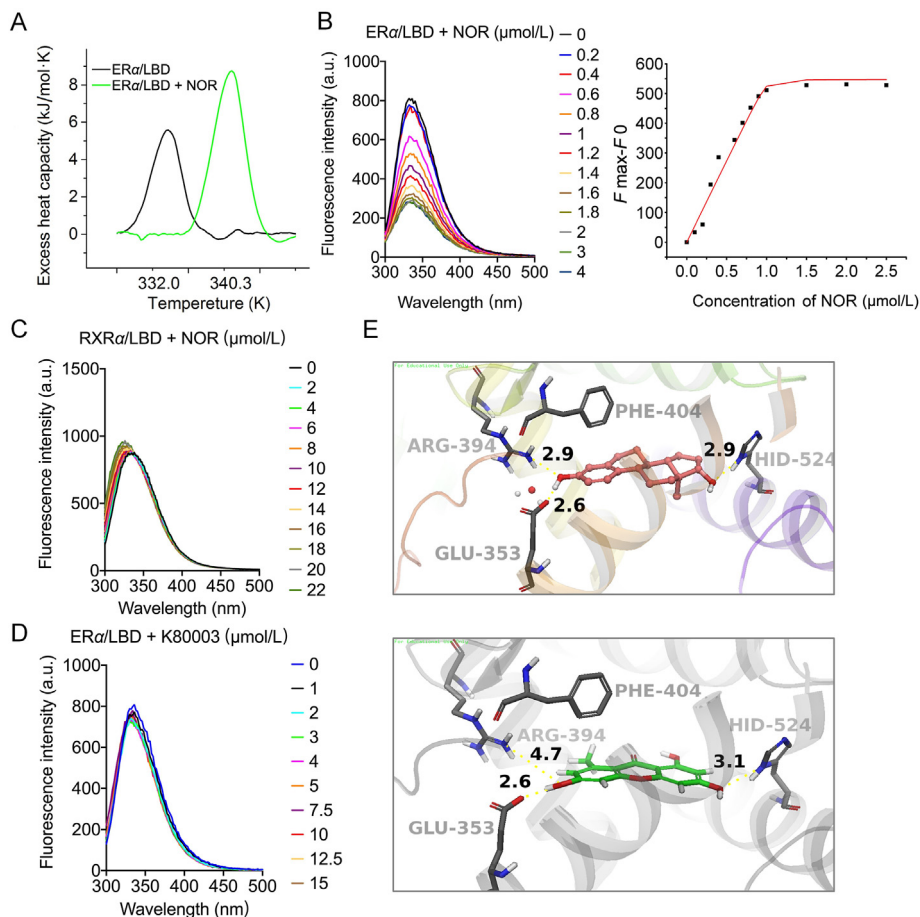
Figure 2 NOR binds to ERα/LBD. (A) Differential scanning calorimetry (DSC) analysis of ERα/LBD protein incubated with DMSO (black curve) or NOR (green curve). Shown are the profiles of heat capacity (Cp) *vs*. temperature at a scan rate of 90 °C/h for the proteins. (B) Fluorescence titration assay of NOR binding to ERα/LBD. NOR was added sequentially to the cuvette with ERα/LBD protein and the fluorescence spectra were recorded for each titration. The excitation wavelength was set to 280 nm, and the emission wavelengths were between 300 and 500 nm. The compound concentration was the abscissa, and the change in spectroscopic signal after each titration was plotted as the ordinate (left panel). The Origin software and the formula $y = C (x + P + K_d)/2 - C \times$ sqrt $((x + P + K_d)^2 - 4Px)/2$ was used to calculate the K_d (right panel). (C) and (D) Fluorescence titration assays of NOR binding to RXRα/LBD (C) and K-80003 binding to ERα/LBD (D). (E) The ERα binding modes of E_2 (up panel) and NOR (down panel) were mimicked by computer-aided docking approach. The structures of E_2 and NOR are shown in orange and green, respectively. The docking scores of E_2 and NOR are −10.607 and −9.298, respectively.
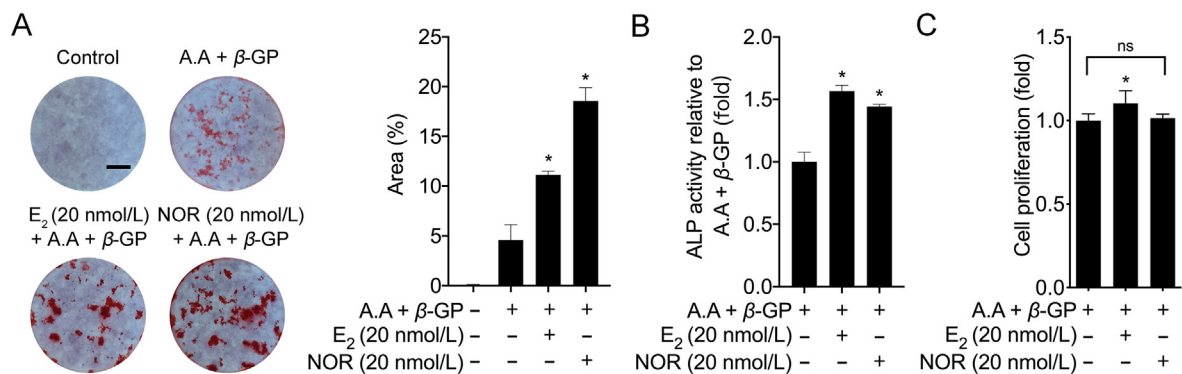

Figure 3 NOR induces osteoblastic differentiation. (A) and (B) MC3T3-E1 cells were treated with mineralization-inducing solution including 10 mmol/L of β-glycerophosphate (β-GP) and 50 μg/mL of ascorbic acid (A.A) together with E_2 or NOR. After 14 days, cells were stained with alizarin red and photographed (A, left panel), and the percentages of the red areas in the total areas were measured and plotted (A, right panel); or cells were lysed and the activities of alkaline phosphatase (ALP) were measured and plotted (B). Scale bar represents 0.3 cm. (C) MC3T3-E1 cells were incubated with mineralization-inducing solution together with E_2 or NOR for 72 h. Cell viability were determined by MTT assay. Data are expressed as the mean ± SD; *$P < 0.05$ by Student's *t* test.
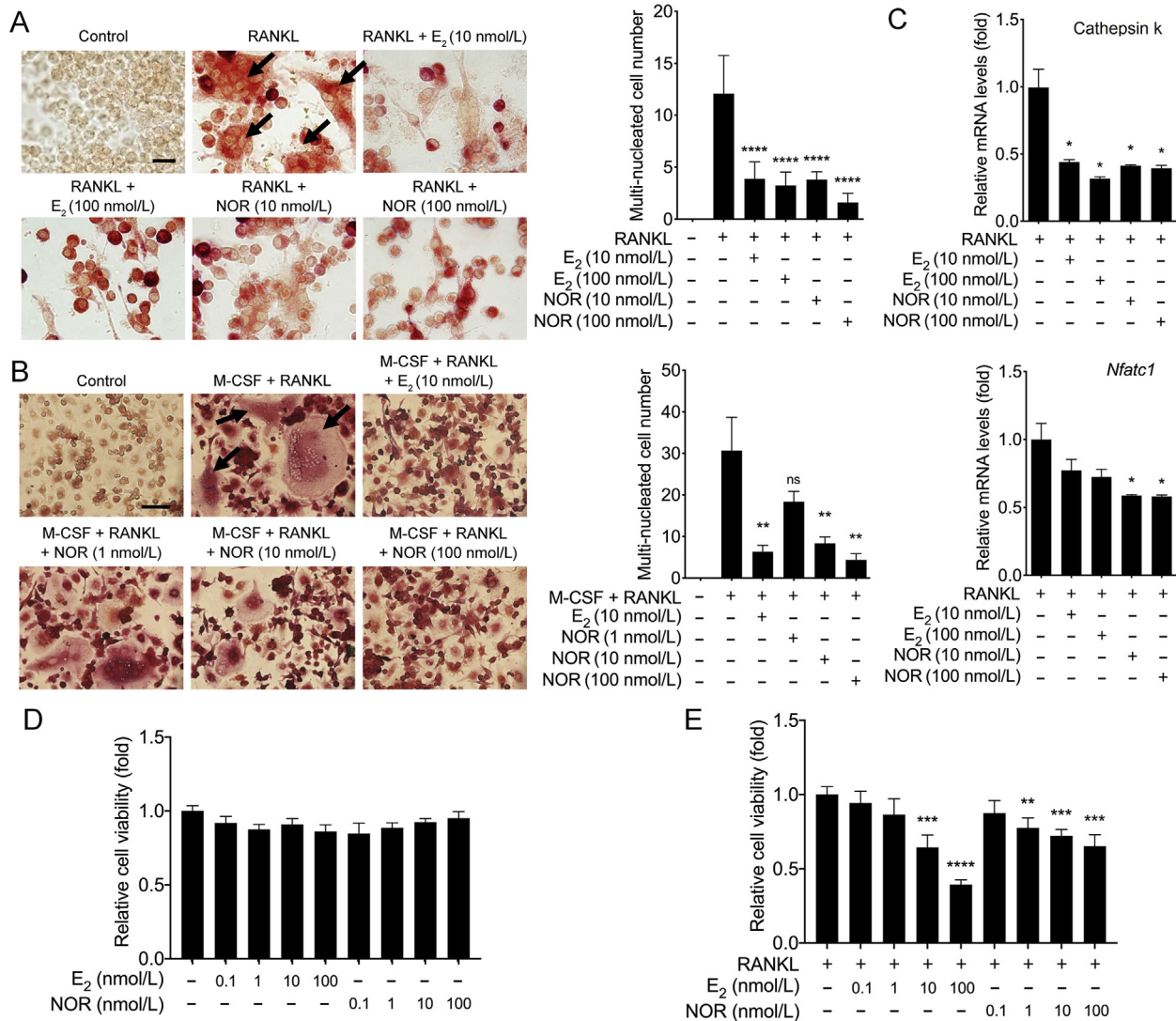
Figure 4 NOR attenuates RANKL-induced osteoclast formation *in vitro*. (A) RAW264.7 cells were treated with RANKL (50 ng/mL) together with E_2 or NOR for 7 days. Cells were then fixed and the tartrate-resistant acid phosphatase (TRAP) staining was applied to identify TRAP-positive multi-nucleated cells. Images were acquired at $100 \times$ magnification on a microscope (left panel). Black arrows indicate the induced multi-nucleated cells. Scale bar represents 20 μm. The numbers of TRAP-positive multi-nucleated cells in a $4 \times$ microscope field of view were counted and presented (right panel). (B) Monocytes purified from bone marrows of C57BL/6 mice were stimulated with 50 ng/mL of RANKL and 50 ng/mL of M-CSF together with E_2 or NOR for 7 days and then stained for TRAP (left panel). Images were acquired at $20 \times$ magnification on a microscope (left panel). Black arrows indicate the induced multi-nucleated cells. Scale bar represents 100 μm. The numbers of TRAP-positive multi-nucleated cells in a well of a 96-well plate were counted and presented (right panel). (C) RAW264.7 cells were stimulated with RANKL (50 ng/mL) in the presence or absence of different doses of E_2 or NOR for 72 h. The mRNA expression of cathepsin K and *Nfatc-1* were detected by quantitative real-time PCR. (D) RAW264.7 cells were treated with NOR or E_2 at the indicated concentrations for 72 h. Cell viability were determined by MTT assay. (E) RAW264.7 cells were pretreated with 50 ng/mL RANKL for 72 h, and then treated with NOR or E_2 together with RANKL for 72 h. Cell viability were determined by MTT assay. Data are expressed as the mean $\pm$ SD; $*P < 0.05$; $**P < 0.01$; $***P < 0.001$; $****P < 0.0001$ by Student's *t* test.

ovariectomy. Treatment with E_2 at 1 mg/kg dosage could rescue OVX-induced uterine shrinkage and weight loss. Even more, the uterine weight of E_2-treated OVX mice was much higher than that of sham mice (Fig. 7A and Fig. S8A), exhibiting the strong potency of E_2 in uterine stimulation. However, NOR at the dosage of 1 mg/kg failed to show apparent effect on morphological change and weight increase of uterus in OVX mice (Fig. 7A and Fig. S8A), indicating the weak estrogenic potency of NOR in uterus.

Treatment with E_2 strongly promoted proliferation and cell cycle progression of MCF-7 but not ERα-null MDA-MB-231 cells (Fig. 7B and C, Fig. S8B and S8C), verifying the onco-promotive effect of E_2 on breast cancer in an ERα-dependent manner. However, NOR failed to show strong effect as E_2 on cell cycle progression and proliferation of either MCF-7 or MDA-MB-231 cells (Fig. 7B and C, Fig. S8B and S8C), indicating the weak effect of NOR on breast cancer promotion. Therefore, these results indicate that NOR is of weak estrogenic activity.
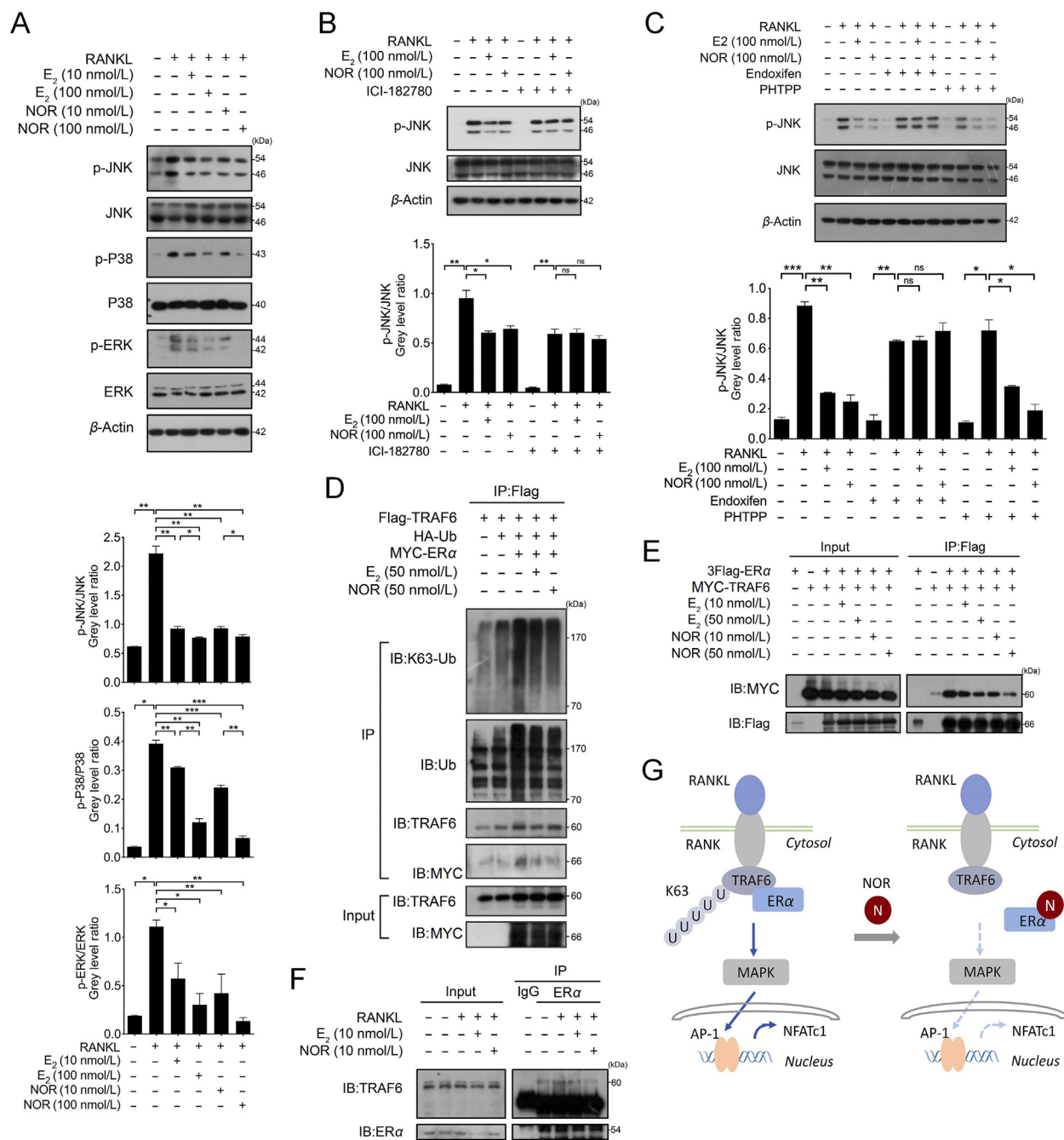
Figure 5 NOR suppresses RANKL signaling by preventing ERα-induced TRAF6 ubiquitination. (A) RAW264.7 cells were pretreated with E₂ or NOR for 4 h and subsequently stimulated with RANKL (50 ng/mL) for 20 min. Cell lysates were subjected to Western blotting analysis of the phosphorylation of JNK, P38 and ERK. The bands of phosphorylated proteins and their corresponding total proteins were quantified by Image J, and the ratio was plotted. (B) and (C) RAW264.7 cells were pretreated with ICI-182780 (1 μmol/L), endoxifen (0.2 μmol/L) or PHTPP (0.2 μmol/L) for 24 h and then treated with E₂ or NOR for 4 h before RANKL (50 ng/mL) stimulation for 20 min. Western blotting was applied to detect protein expression. The gray level of p-JNK bands were normalized to that of total JNK bands. (D) HEK293T cells were co-transfected with the indicated expression plasmids for 24 h and then treated with E₂ or NOR for 2 h. Flag-TRAF6 was immunoprecipitated by anti-Flag antibody, and Lys63-linked and total ubiquitination of TRAF6 were examined by Western blotting using anti-K63-linked-ubiquitin and anti-ubiquitin antibodies, respectively. (E) HEK293T cells were co-transfected with Flag-ERα and MYC-TRAF6 expression plasmids for 24 h, followed by treatment with E₂ or NOR for 2 h. Protein interactions were examined by immunoprecipitation using anti-Flag antibody and Western blotting using anti-MYC antibody. (F) RAW264.7 cells were pretreated with E₂ or NOR for 2 h and subsequently stimulated with RANKL (50 ng/mL) for 20 min. Protein interactions were examined by immunoprecipitation using anti-ERα antibody and Western blotting using anti-TRAF6 antibody. Normal IgG was as an immunoprecipitation control. (G) Working model of ERα and NOR in RANKL signaling. Data were expressed as the mean ± SD; ns, non-significant; *$P < 0.05$; **$P < 0.01$; ***$P < 0.001$ by Student's t test.
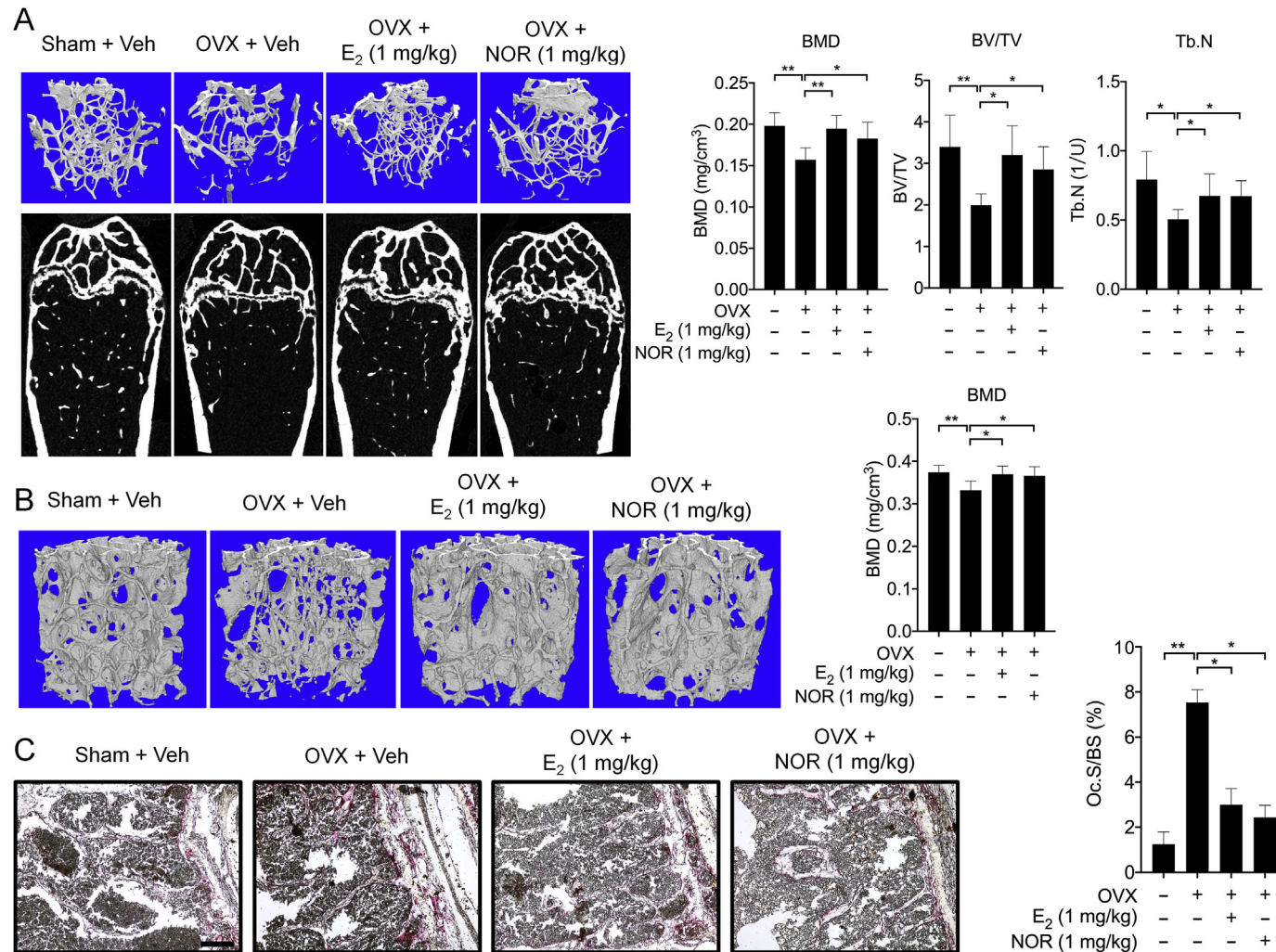
Figure 6 NOR ameliorates ovariectomy-induced bone loss *in vivo*. Female mice were subjected to bilateral ovariectomy (OVX) or sham operation (Sham). NOR and E_2 were administered orally for 8 weeks. Mice were then sacrificed. Mouse femurs (A) and the 5th vertebras (B) were analyzed by micro-CT and the 3D reconstructions of trabecular were obtained using the software CTAn. The bone mineral density (BMD), bone volume density (BV/TV) and trabecular number (Tb.N) were determined by the scanner software. The 5th vertebras were sliced into 5-μm thick sections to perform tartrate-resistant acid phosphatase (TRAP) staining (C). Scale bar represents 200 μm. The osteoclast surface (Oc.S) and bone surface (BS) of TRAP-stained histologic sections of vertebra were respectively measured by Image J, and the fold change in osteoclast surface/bone surface (Oc.S/BS) was analyzed by GraphPad Prism 8 (C). Data are expressed as the mean ± SD, $n = 6$; *$P < 0.05$; **$P < 0.01$ by Student's t test.
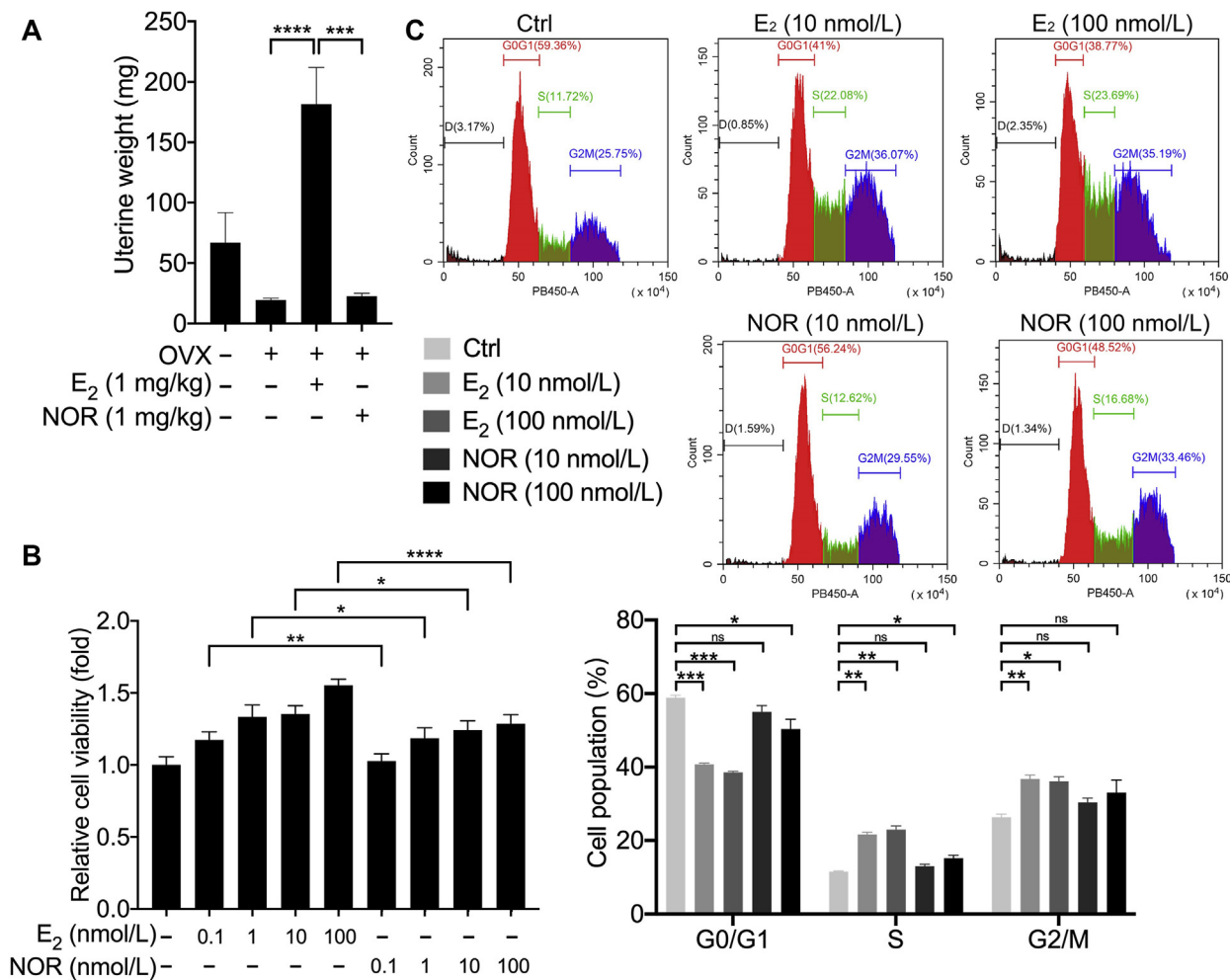
Figure 7 NOR is of weak estrogenic activity. (A) Weights of uterus from Sham and OVX mice treated with E_2 or NOR for 8 weeks. (B) MCF-7 cells were treated with E_2 or NOR for 48 h. MTT assay was performed to examine cell proliferation. (C) MCF-7 cells were treated with E_2 or NOR for 24 h. The cell cycles were detected by flow cytometry analysis. Data were expressed as the mean ± SD; ns, non-significant; *$P < 0.05$; **$P < 0.01$; ***$P < 0.001$; ****$P < 0.0001$ by Student's t test.

4. Discussion

Discovering and dissecting novel ligands of ERα from natural products would not only provide potential drugs for ERα-related diseases, but also aid to reveal novel mechanisms of ERα activities. Here, we used ERα mammalian one-hybrid assay to screen for ERα modulators from plant endophytes and successfully identified NOR as an active ligand of ERα. Our ligand-receptor binding assay revealed the nanomolar range of ERα binding affinity of NOR. Moreover, NOR at nmol/L concentrations was able to regulate ERα transcriptional activity, osteoblast/osteoclast formation and RANKL signaling. These results indicate that NOR is a high-affinity ligand of ERα and a high-potency modulator of some biological activities, which guarantees the further exploration of ERα-dependent activities of NOR and the further optimization of NOR for drug development. The structure of NOR is distinct from the clinical ERα-targeted drugs, which lies down the foundation to develop NOR for regulating distinct ERα-related pathological processes. Moreover, NOR and its optimized derivatives may overcome the resistance or adverse effects of current clinical ERα-targeted drugs.

Our results reveal that NOR is of strong effect in osteoporosis prevention. We found that NOR not only induced osteoblast formation but also prevented osteoclast formation. Notably, the above capability of NOR was comparable to E_2. As for osteoclast formation, NOR not only inhibited osteoclastic differentiation, indicating from NOR-induced decrease of osteoclast formation from precursor cells, but also inhibited osteoclast growth or survival, indicating from NOR-induced viability decrease of RANKL-pretreated RAW264.7 cells. RANKL signaling is essential for inducing osteoclastic differentiation as well as for maintaining osteoclast survival and growth[52]. Indeed, we found that NOR potently inhibited RANKL signaling, revealing the underlying mechanism of osteoclastic inhibition by NOR. Furthermore, we revealed that ERα was able to interact with TRAF6 and induce its Lys63-linked ubiquitination, demonstrating the positive role of ERα in RANKL signaling. Importantly, NOR potently inhibited ERα-induced TRAF6 ubiquitination and RANKL-induced interaction of ERα and TRAF6, resulting in down-regulation of RANKL signaling. Thus, our study unraveled a non-genomic action of ERα in regulating RANKL signaling, which was negatively regulated by NOR.

The pivotal role of TRAF6 in transducing RANKL signaling confers it an attractive drug target for modulating RANKL signaling[53]. Downregulation of its expression and activity will inhibit RANKL signaling and thereby inhibit RANKL-induced osteoclastogenesis. It has been reported that icaritin, a natural prenylflavonoid, inhibits RANKL signaling by inducing TRAF6 poly-ubiquitination and proteasomal degradation[29]. We also found that NOR inhibited RANKL signaling. However, we did not observe significant effect of NOR on decreasing TRAF6 protein level. Whereas Lys48-linked poly-ubiquitination results in TRAF6 degradation, Lys63-linked poly-ubiquitination activates TRAF6 in RANKL signaling[24,49,54]. Indeed, we found that NOR strongly inhibited ERα-induced Lys63-linked ubiquitination of TRAF6. Thus, instead of downregulation of TRAF6 expression, NOR was able to inhibit TRAF6 activation to antagonize RANKL signaling. Notably, we found that NOR acted through targeting ERα, which may provide an approach for interfering TRAF6 activity by small molecules targeting ERα.

E_2 has been shown to downregulate RANKL expression likely through transcriptional regulation to inhibit RANKL signaling[46,55]. However, in our cell model this mechanism was excluded because we used exogenous RANKL to stimulate the signaling pathway. Thus, the genomic and non-genomic actions of E_2 might both contribute to its inhibition of RANKL signaling and osteoclastogenesis. Whereas NOR possessed weaker ability than E_2 in regulating ERα transactivation, it was of the comparable ability as E_2 in inhibiting RANKL signaling and osteoclast formation. Thus, the regulation of non-genomic actions of ERα by some ligands, such as NOR, may produce enough benefit for osteoporosis. Development of ERα biased ligands with strong regulation of ERα non-genomic activity but weak regulation of ERα transactivation might dissociate the beneficial effect of ERα targeting from some adverse effects.

One major concern of estrogen in osteoporosis treatment is to increase the risk of endometrial, ovarian and mammary carcinoma, although clinical studies have proven that longtime and low-dose HRT has no significant risk of these carcinomas[56]. We found that NOR was of much low ability in promoting MCF-7 proliferation and restoring the ovariectomy-induced loss of uterine weight. This indicate the much less risk of NOR than E_2 in promoting estrogen-related carcinomas. The less estrogenic activity of NOR might result from its lower ability of inducing ERα transactivation or its tissue-selective activation property. However, further detailed investigation should be performed to verify the safety of NOR in osteoporosis treatment.

5. Conclusions

Collectively, our study demonstrates that natural product NOR, purified from plant endophyte, is a high-affinity ligand of ERα and a potential drug lead for prevention and treatment of postmenopausal osteoporosis. Moreover, we reveal the positive role and non-genomic action of ERα in RANKL signaling and the underlying mechanism of osteoclastic inhibition of NOR *via* targeting ERα.

Acknowledgments

Author contributions

Conflicts of interest

The authors declare that they have no conflict of interest.

Appendix A. Supporting information

Supporting data to this article can be found online at https://doi.org/10.1016/j.apsb.2020.09.012.

References

1. Schild-Hay LJ, Leil TA, Divi RL, Olivero OA, Weston A, Poirier MC. Tamoxifen induces expression of immune response-related genes in cultured normal human mammary epithelial cells. *Canc Res* 2009;**69**:1150−5.
2. Robinson-Rechavi M, Escriva Garcia H, Laudet V. The nuclear receptor superfamily. *J Cell Sci* 2003;**116**:585−6.
3. Melville KM, Kelly NH, Surita G, Buchalter DB, Schimenti JC, Main RP, et al. Effects of deletion of er-alpha in osteoblast-lineage cells on bone mass and adaptation to mechanical loading differ in female and male mice. *J Bone Miner Res* 2015;**30**:1468−80.
4. Ribas V, Drew BG, Zhou Z, Phun J, Kalajian NY, Soleymani T, et al. Skeletal muscle action of estrogen receptor α is critical for the maintenance of mitochondrial function and metabolic homeostasis in females. *Sci Transl Med* 2016;**8**:334ra54.
5. Burns KA, Korach KS. Estrogen receptors and human disease: an update. *Arch Toxicol* 2012;**86**:1491−504.
6. Puranik NV, Srivastava P, Bhatt G, John Mary DJS, Limaye AM, Sivaraman J. Determination and analysis of agonist and antagonist potential of naturally occurring flavonoids for estrogen receptor (ERα) by various parameters and molecular modelling approach. *Sci Rep* 2019;**9**:7450.
7. Gehm BD, McAndrews JM, Chien PY, Jameson JL. Resveratrol, a polyphenolic compound found in grapes and wine, is an agonist for the estrogen receptor. *Proc Natl Acad Sci U S A* 1997;**94**:14138−43.
8. Bialesova L, Brtko J, Lenko V, Macejova D. Nuclear receptors—target molecules for isoflavones in cancer chemoprevention. *Gen Physiol Biophys* 2013;**32**:467−78.
9. Smiley DA, Khalil RA. Estrogenic compounds, estrogen receptors and vascular cell signaling in the aging blood vessels. *Curr Med Chem* 2009;**16**:1863−87.

10. Selective estrogen receptor modulators. In: *Livertox: clinical and research information on drug-induced liver injury.* Bethesda: National Institute of Diabetes and Digestive and Kidney Diseases; 2012.

11. Khosla S, Oursler MJ, Monroe DG. Estrogen and the skeleton. *Trends Endocrinol Metab* 2012;**23**:576−81.

12. Watts NB. Postmenopausal osteoporosis: a clinical review. *J Womens Health (Larchmt)* 2018;**27**:1093−6.

13. Siddiqui JA, Partridge NC. Physiological bone remodeling: systemic regulation and growth factor involvement. *Physiology* 2016;**31**:233−45.

14. Cauley JA. Estrogen and bone health in men and women. *Steroids* 2015;**99**:11−5.

15. Nakamura T, Imai Y, Matsumoto T, Sato S, Takeuchi K, Igarashi K, et al. Estrogen prevents bone loss *via* estrogen receptor α and induction of fas ligand in osteoclasts. *Cell* 2007;**130**:811−23.

16. Ohta H. Bone metabolism and cardiovascular function update. Estrogen and its therapeutic potential for bone and vascular health. *Clin Calcium* 2014;**24**:107−15.

17. Khosla S, Hofbauer LC. Osteoporosis treatment: recent developments and ongoing challenges. *Lancet Diabetes Endocrinol* 2017;**5**:898−907.

18. Camacho PM, Petak SM, Binkley N, Clarke BL, Harris ST, Hurley DL, et al. American association of clinical endocrinologists and American college of endocrinology clinical practice guidelines for the diagnosis and treatment of postmenopausal osteoporosis−2016. *Endocr Pract* 2016;**22**:1−42.

19. Khan M, Cheung AM, Khan AA. Drug-related adverse events of osteoporosis therapy. *Endocrinol Metab Clin North Am* 2017;**46**:181−92.

20. Corsi A, Ungari C, Riminucci M, Agrillo A. Bisphosphonate-related osteonecrosis and metastasis within the same site of the Jaw. *J Oral Maxillofac Surg* 2017;**75**:1679−84.

21. Herrero S, Pico Y. Treatments for post-menopausal osteoporotic women, what's new? How can we manage long-term treatment?. *Eur J Pharmacol* 2016;**779**:8−21.

22. Gambacciani M, Levancini M. Hormone replacement therapy and the prevention of postmenopausal osteoporosis. *Prz Menopauzalny* 2014;**13**:213−20.

23. Rossouw JE, Anderson GL, Prentice RL, LaCroix AZ, Kooperberg C, Stefanick ML, et al. Risks and benefits of estrogen plus progestin in healthy postmenopausal women: principal results from the women's health initiative randomized controlled trial. *J Am Med Assoc* 2002;**288**:321−33.

24. Lamothe B, Webster WK, Gopinathan A, Besse A, Campos AD, Darnay BG. TRAF6 ubiquitin ligase is essential for RANKL signaling and osteoclast differentiation. *Biochem Biophys Res Commun* 2007;**359**:1044−9.

25. He X, Andersson G, Lindgren U, Li Y. Resveratrol prevents RANKL-induced osteoclast differentiation of murine osteoclast progenitor RAW 264.7 cells through inhibition of ROS production. *Biochem Biophys Res Commun* 2010;**401**:356−62.

26. Teitelbaum SL, Ross FP. Genetic regulation of osteoclast development and function. *Nat Rev Genet* 2003;**4**:638−49.

27. Sobacchi C, Menale C, Villa A. The RANKL−RANK axis: a bone to thymus round trip. *Front Immunol* 2019;**10**:629.

28. Wada T, Nakashima T, Hiroshi N, Penninger JM. RANKL−RANK signaling in osteoclastogenesis and bone disease. *Trends Mol Med* 2006;**12**:17−25.

29. Tan EM, Li L, Indran IR, Chew N, Yong EL. TRAF6 mediates suppression of osteoclastogenesis and prevention of ovariectomy-induced bone loss by a novel prenylflavonoid. *J Bone Miner Res* 2017;**32**:846−60.

30. Lomaga MA, Yeh WC, Sarosi I, Duncan GS, Furlonger C, Ho A, et al. TRAF6 deficiency results in osteopetrosis and defective interleukin-1, CD40, and LPS signaling. *Genes Dev* 1999;**13**:1015−24.

31. Walsh MC, Choi Y. Biology of the RANKL−RANK−OPG system in immunity, bone, and beyond. *Front Immunol* 2014;**5**:511.

32. Robinson LJ, Yaroslavskiy BB, Griswold RD, Zadorozny EV, Guo L, Tourkova IL, et al. Estrogen inhibits RANKL-stimulated osteoclastic differentiation of human monocytes through estrogen and RANKL-regulated interaction of estrogen receptor-alpha with BCAR1 and TRAF6. *Exp Cell Res* 2009;**315**:1287−301.

33. Kusari S, Hertweck C, Spiteller M. Chemical ecology of endophytic fungi: origins of secondary metabolites. *Chem Biol* 2012;**19**:792−8.

34. Aly AH, Debbab A, Proksch P. Fungal endophytes: unique plant inhabitants with great promises. *Appl Microbiol Biotechnol* 2011;**90**:1829−45.

35. Stierle A, Strobel G, Stierle D. Taxol and taxane production by taxomyces andreanae, an endophytic fungus of pacific yew. *Science* 1993;**260**:214−6.

36. Chen L, Aleshin AE, Alitongbieke G, Zhou Y, Zhang X, Ye X, et al. Modulation of nongenomic activation of PI3K signalling by tetramerization of N-terminally-cleaved RXRα. *Nat Commun* 2017;**8**:16066.

37. Ren G, Bao W, Zeng Z, Zhang W, Shang C, Wang M, et al. RXRα nitro-ligand Z-10 and its optimized derivative Z-36 reduce β-amyloid plaques in Alzheimer's disease mouse model. *Mol Pharm* 2019;**16**:480−8.

38. Kurganov BI, Lyubarev AE, Sanchez-Ruiz JM, Shnyrov VL. Analysis of differential scanning calorimetry data for proteins. criteria of validity of one-step mechanism of irreversible protein denaturation. *Biophys Chem* 1997;**69**:125−35.

39. Stauffer SR, Coletta CJ, Tedesco R, Nishiguchi G, Carlson K, Sun J, et al. Pyrazole ligands: structure-affinity/activity relationships and estrogen receptor-alpha-selective agonists. *J Med Chem* 2000;**43**:4934−47.

40. Xiao HH, Gao QG, Ho MX, Zhang Y, Wong KC, Dai Y, et al. An 8-*O*-4′ norlignan exerts oestrogen-like actions in osteoblastic cells *via* rapid nongenomic ER signaling pathway. *J Ethnopharmacol* 2015;**170**:39−49.

41. Lee DH, Jeon EJ, Ahn J, Hwang JT, Hur J, Ha TY, et al. Limonin enhances osteoblastogenesis and prevents ovariectomy-induced bone loss. *J Funct Food* 2016;**23**:105−14.

42. Maeda T, Matsunuma A, Kawane T, Horiuchi N. Simvastatin promotes osteoblast differentiation and mineralization in MC3T3-E1 cells. *Biochem Biophys Res Commun* 2001;**280**:874−7.

43. Jiang M, Wang T, Yan X, Liu Z, Yan Y, Yang K, et al. A novel rhein derivative modulates bone formation and resorption and ameliorates estrogen-dependent bone loss. *J Bone Miner Res* 2019;**34**:361−74.

44. Kim KJ, Yeon JT, Choi SW, Moon SH, Ryu BJ, Yu R, et al. Decursin inhibits osteoclastogenesis by downregulating NFATc1 and blocking fusion of pre-osteoclasts. *Bone* 2015;**81**:208−16.

45. Lee W, Ko KR, Kim HK, Lee DS, Nam IJ, Lim S, et al. Dehydrodiconiferyl alcohol inhibits osteoclast differentiation and ovariectomy-induced bone loss through acting as an estrogen receptor agonist. *J Nat Prod* 2018;**81**:1343−56.

46. Shevde NK, Bendixen AC, Dienger KM, Pike JW. Estrogens suppress RANK ligand-induced osteoclast differentiation *via* a stromal cell independent mechanism involving c-Jun repression. *Proc Natl Acad Sci U S A* 2000;**97**:7829−34.

47. Wu X, Hawse JR, Subramaniam M, Goetz MP, Ingle JN, Spelsberg TC. The tamoxifen metabolite, endoxifen, is a potent antiestrogen that targets estrogen receptor alpha for degradation in breast cancer cells. *Canc Res* 2009;**69**:1722−7.

48. Ogo Y, Taniuchi S, Ojima F, Hayashi S, Murakami I, Saito Y, et al. *IGF-1* gene expression is differentially regulated by estrogen receptors α and β in mouse endometrial stromal cells and ovarian granulosa cells. *J Reprod Dev* 2014;**60**:216−23.

49. Kanayama A, Seth RB, Sun L, Ea CK, Hong M, Shaito A, et al. TAB2 and TAB3 activate the NF-kappaB pathway through binding to polyubiquitin chains. *Mol Cell* 2004;**15**:535−48.

50. Komori T. Animal models for osteoporosis. *Eur J Pharmacol* 2015;**759**:287−94.

51. Hsueh AJ, Erickson GF, Lu KH. Changes in uterine estrogen receptor and morphology in aging female rats. *Biol Reprod* 1979;**21**:793−800.

52. Zhao Y, Wang HL, Li TT, Yang F, Tzeng CM. Baicalin ameliorates dexamethasone-induced osteoporosis by regulation of the RANK/RANKL/OPG signaling pathway. *Drug Des Devel Ther* 2020;**14**:195−206.

53. Gohda J, Akiyama T, Koga T, Takayanagi H, Tanaka S, Inoue J. RANK-mediated amplification of TRAF6 signaling leads to NFATC1 induction during osteoclastogenesis. *EMBO J* 2005;**24**:790−9.

54. Lamothe B, Besse A, Campos AD, Webster WK, Wu H, Darnay BG. Site-specific Lys-63-linked tumor necrosis factor receptor-associated factor 6 auto-ubiquitination is a critical determinant of I kappa B kinase activation. *J Biol Chem* 2007;**282**:4102−12.

55. Streicher C, Heyny A, Andrukhova O, Haigl B, Slavic S, Schüler C, et al. Estrogen regulates bone turnover by targeting RANKL expression in bone lining cells. *Sci Rep* 2017;**7**:6460.

56. Langer RD. Efficacy, safety, and tolerability of low-dose hormone therapy in managing menopausal symptoms. *J Am Board Fam Med* 2009;**22**:563−73.